AMERICAN SOCIETY FOR MICROBIOLOGY | Molecular and Cellular Biology®

RESEARCH ARTICLE

MBD4 Facilitates Immunoglobulin Class Switch Recombination

Fernando Grigera, Robert Wuerffel, Amy L. Kenter

Department of Microbiology and Immunology, University of Illinois College of Medicine, Chicago, Illinois, USA

ABSTRACT Immunoglobulin heavy chain class switch recombination (CSR) requires targeted formation of DNA double-strand breaks (DSBs) in repetitive switch region elements followed by ligation between distal breaks. The introduction of DSBs is initiated by activation-induced cytidine deaminase (AID) and requires base excision repair (BER) and mismatch repair (MMR). The BER enzyme methyl-CpG binding domain protein 4 (MBD4) has been linked to the MMR pathway through its interaction with MutL homologue 1 (MLH1). We find that when *Mbd4* exons 6 to 8 are deleted in a switching B cell line, DSB formation is severely reduced and CSR frequency is impaired. Impaired CSR can be rescued by ectopic expression of *Mbd4*. *Mbd4* deficiency yields a deficit in DNA end processing similar to that found in MutS homologue 2 (*Msh2*)- and *Mlh1*-deficient B cells. We demonstrate that microhomology-rich S-S junctions are enriched in cells in which *Mbd4* is deleted. Our studies suggest that *Mbd4* is a component of MMR-directed DNA end processing.

KEYWORDS Ig class switch recombination, mismatch repair, B cells, Ig class switch, uracil glycosylase

Received 2 June 2016 **Returned for modification** 16 August 2016 **Accepted** 30 September 2016

Accepted manuscript posted online 24 October 2016

Citation Grigera F, Wuerffel R, Kenter AL. 2017. MBD4 facilitates immunoglobulin class switch recombination. Mol Cell Biol 37:e00316-16. https://doi.org/10.1128/MCB.00316-16.

Address correspondence to Amy L. Kenter, star1@uic.edu.

The immunoglobulin (Ig) diversification reactions somatic hypermutation (SHM) and class switch recombination (CSR) are initiated by activation-induced deaminase (AID) in mature B lymphocytes. CSR involves intrachromosomal deletional rearrangements that swap the default μ constant (C_H) region for one of six different downstream C_H regions (γ3, γ1, γ2b, γ2a, ε, and α), but not Cδ, while preserving the antigen binding specificity of V(D)J exons. CSR is focused to specific switch (S) regions by differential activation of germ line transcription that traverses a noncoding intervening (I) exon, an S region, and a C_H coding region (1, 2). During CSR, two S regions, each paired with a C_H region, are brought into close proximity by long-range chromatin interactions that are anchored by transcriptional elements (3). AID initiates CSR by creating DNA lesions in donor Sμ and downstream acceptor S regions that are processed into DNA double-strand breaks (DSBs) and used in the recombination reaction (4).

The conversion of AID-induced damage into DSBs is mediated primarily through base excision repair (BER) (5). AID deaminates dC, producing uracil, which is processed into an abasic site by uracil DNA glycosylase (UNG); the abasic site is then cleaved by apurinic/apyrimidinic endonuclease (APE) to generate a single-strand break (SSB) (6). Closely spaced SSBs on cDNA strands will be processed into DSBs. UNG deficiency in mice (5) and humans (7) leads to severely compromised CSR and to perturbed SHM. AID-induced DSBs occur primarily in G_1 phase (8), ensuring that break resolution occurs through classical nonhomologous end joining (NHEJ) DNA repair (9). AID and UNG deficiencies also lead to a dramatic reduction in S region specific breaks, indicating that DSB formation is central to the mechanism of CSR (10). Mismatch repair (MMR) functions as an alternative pathway for DSB formation during CSR. MMR deficiencies of Msh2, Msh6, Pms2, Mlh1, and exonuclease I (Exol) in mice contribute to a 2- to 7-fold reduction in CSR (reviewed in reference 6). MMR becomes involved when AID-induced

uracils are too distantly spaced on complementary strands to permit processing by BER. However, many aspects of CSR-related DSB formation and processing remain unclear.

There are four uracil DNA glycosylases, UNG, SMUG1, TDG, and methyl-CpG binding domain protein 4 (MBD4), that recognize and remove dU in U-G mismatches (11). Although SMUG1 and TDG play no role in these processes when UNG is intact (12–14), SMUG can partially support CSR in UNG-deficient cells (14). We were intrigued by the functional association of MBD4 and AID in active DNA demethylation in zebrafish (15). Moreover, MBD4 interacts with MLH1 (16) and PMS2 (17) and might directly contribute to the removal of U-G mismatches in collaboration with the MMR pathway (18). Unexpectedly, CSR was not affected by targeted deletion of *Mbd4* exon 3 (19) or exons 2 to 5 (termed *Mbd4*$^{\Delta 2\text{-}5/\Delta 2\text{-}5}$) (17) in mice. However, we now show that targeted deletion of *Mbd4* 5′ exons permits variant transcript expression from the intact 3′ end of the locus. Furthermore, two MBD4 isoforms, the full-length (FL) and short-form (SF) isoforms, are detected in wild-type (WT) B cells. Although FL MBD4 is absent in *Mbd4*$^{\Delta 2\text{-}5/\Delta 2\text{-}5}$ B cells, the SF is present, indicating that expression is not fully abolished and may complicate functional analyses. These findings have prompted us to reconsider a role for *Mbd4* in CSR and its contribution to S region DSB formation.

Here we report the construction of CH12 cell lines with deletions of (i) *Mbd4* exons 6 to 8 and (ii) exon 8 through the 3′ untranslated region (UTR) in which expression of FL and SF MBD4 is abolished and CSR is impaired. The CSR deficit is rescued by ectopic expression of truncated *Mbd4* exons 4 to 8 and is dependent on uracil DNA glycosylase activity. The level of formation of S region DSBs is severely diminished in *Mbd4* knockout (KO) cells relative to that in controls, and these DSBs have characteristics in common with DSBs from MMR-deficient B cells. Rare Sμ-Sα junctions from CSR-activated *Mbd4* KO cells have longer than average microhomologies, characteristic of *Mlh1*-deficient mice. Our data suggest that MBD4 is mechanistically linked to a critical step in DSB formation that is required for optimal CSR and that may be epistatic with the MMR pathway.

RESULTS

Murine MBD4 is a 554-amino-acid (554-aa) protein that is expressed in the cytoplasm and imported into the nuclei of splenic B cells and CH12 cells that are induced to undergo CSR (17). MBD4 contains a methyl-CpG-binding domain (MBD), encoded by exons 2 and 3, and a DNA glycosylase domain, encoded by exons 5 to 8 (20, 21). *Mbd4* is expressed to levels approaching that of AID in GC B cells, suggesting a B-cell-specific function (see Fig. S2 in the supplemental material). Transcript analyses indicate that in addition to full-length (FL) *Mbd4* mRNA, encoded by exons 1 to 8, there are several alternative *Mbd4* transcripts that may be splice variants or independent transcripts from alternative transcription start sites (TSSs) (Fig. 1A). The *Mbd4* transcript initiating downstream of exon 3 encompasses exons 5 to 8 (XM_006505683.2) and encodes a 175-aa polypeptide that includes the entire DNA glycosylase domain and may represent an alternative short form (SF) of *Mbd4* (Fig. 1A). Although another *Mbd4* open reading frame (ORF) spans exons 4 to 8, no transcript for these sequences has yet been reported *in vivo*. The *Mbd4* transcript spanning exons 1a to 7 (XM_006505681.2) is reportedly subject to nonsense-mediated decay. An *Mbd4* transcript encompassing exons 6 to 8 (XP_006505746.1) lacks an intact DNA glycosylase catalytic subunit. In summary, two *Mbd4* transcripts, a full-length (FL) and an SF transcript, are capable of expressing the *Mbd4* DNA glycosylase domain.

We assessed the epigenetic landscape of the *Mbd4* locus for the presence of promoter and enhancer elements that might support *Mbd4* SF expression in B lineage cells by leveraging published studies (see Table S1 in the supplemental material). Enhancers are identified by histone H3 acetylated (Ac) lysine 27 (H3K27Ac) modifications, alone and in conjunction with H3K4 methyl 1 (H3K4me1) marks (22, 23), and are frequently enriched for the transcription cofactor Mediator 1 (Med1) (22, 24). Transcriptionally active promoters are marked by H3K4me3 modifications (22). In B cell progenitors and the CH12 cell line, the H3K27Ac, H3K4me1, and H3K4me3 marks and Med1

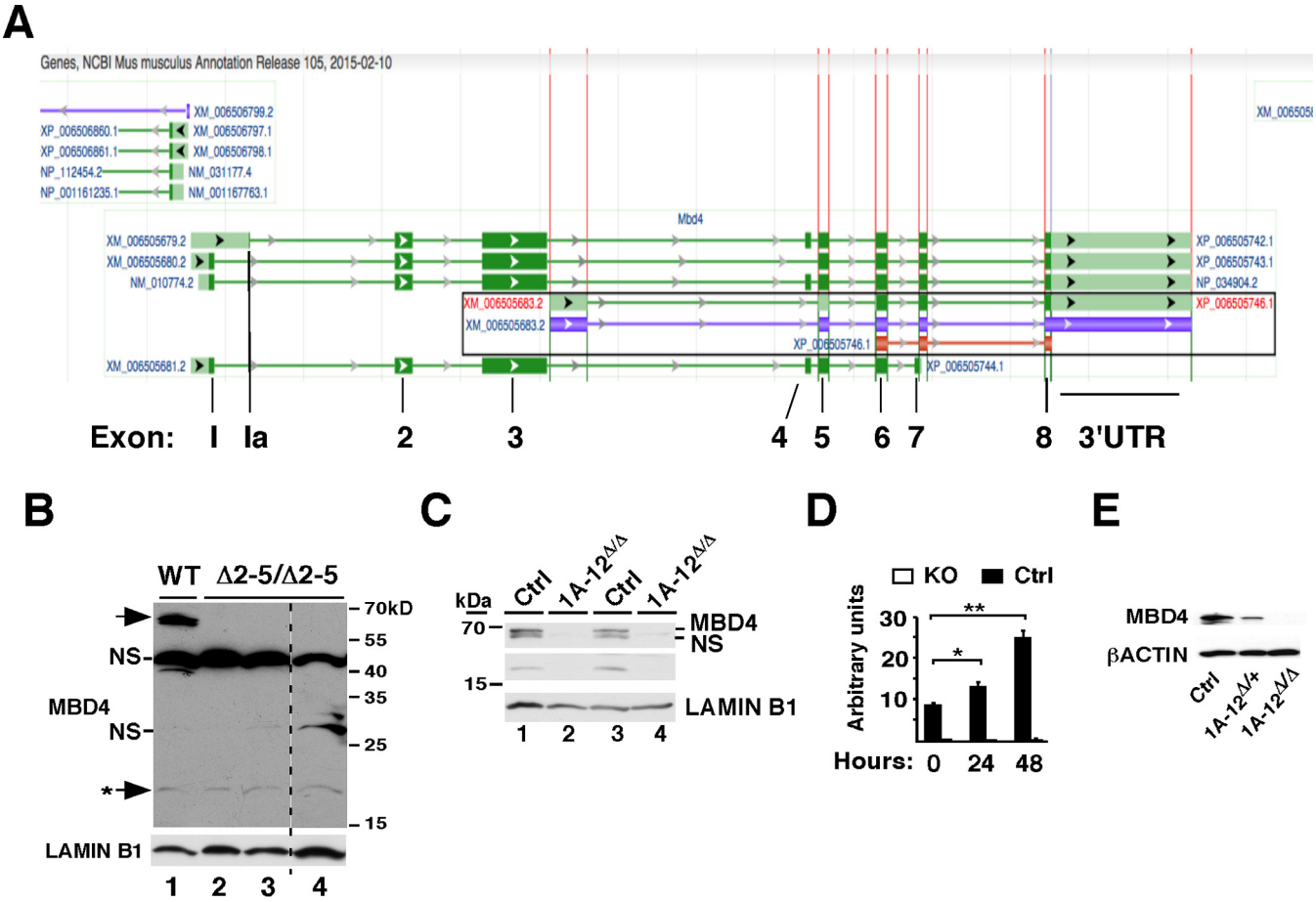

FIG 1 Expression of MBD4 full-length and short isoforms is lost in *Mbd4*-deficient CH12 cells. (A) NCBI browser screenshot of the genomic *Mbd4* locus and a segment of the Ift122 gene. *Mbd4* transcripts are indicated with exons (dark green boxes), untranslated regions (light green boxes), alternative transcripts (red and purple boxes), and introns (lines). (B, C, and E) Western blot analyses of MBD4 protein expression were performed using an antibody against MBD4 (directed against residues in exon 7) and nuclear extracts from WT and *Mbd4*$^{\Delta 2\text{-}5/\Delta 2\text{-}5}$ splenic B cells activated with LPS plus IL-4 for 48 h (B), CH12 control (Ctrl) and *Mbd4* KO (1A-12$^{\Delta/\Delta}$) cells induced by CIT for 24 h (C), and 1A-12$^{+/\Delta}$ cells induced by CIT for 24 h (E). The loading control was developed with anti-lamin B1 or anti-β-actin. (B) Arrows indicate MBD4 full-length (~70-kDa), short-form (~18-kDa) (*), or nonspecific (NS) bands. The dashed line indicates cropping. (C) Control and 1A-12$^{\Delta/\Delta}$ samples are from two independent experiments. (D) *Mbd4* transcripts from control and KO (1A-12$^{\Delta/\Delta}$) cells at 0, 24, and 40 h of CIT treatment were analyzed by qRT-PCR using primers F6.1 and R1 in exon 6 and the 3′ UTR, respectively. *Mbd4* transcript levels were normalized to those for 18S rRNA. The averages from two samples and two independent experiments are shown with SEMs. Asterisks indicate significant differences by Student's two-tailed *t* test (*, $P < 0.05$; **, $P < 0.001$). (E) Western analysis of MBD4 protein expression in CH12 (Ctrl), 1A-12$^{\Delta/\Delta}$, and 1A-12$^{\Delta/+}$ cells.

binding are coincident with *Mbd4* exon 1, indicating the juxtaposition of an enhancer and a promoter that are also occupied by the B cell lineage-specifying transcription factors (TFs) E2A, Pax5, and Ikaros (see Fig. S3 in the supplemental material). Strikingly, the area immediately downstream of exon 3 is enriched both for H3K27Ac and H3K4me1 and for H3K4me3, potentially indicating the presence of a second promoter-and-enhancer pair that could support *Mbd4* SF expression (Fig. S3). However, whether *Mbd4* SF is expressed in activated B cells remains unclear.

Nuclear extracts from activated splenic B cells and the CH12 cell line were subjected to Western blot analyses to test for the presence of distinct MBD4 polypeptides using an anti-MBD4 antibody (Ab) specific for residues in exon 7. Lamin B1 was used as a loading control to confirm the integrity of the nuclear extracts (Fig. 1B and C). FL (~70-kDa) and SF (~18-kDa) MBD4 polypeptides are induced in the nuclei of activated splenic B cells and upon induction of CH12 cells with CD40 ligand (CD40L) plus interleukin 4 (IL-4) plus transforming growth factor β (TGF-β) (CIT) (Fig. 1B, lane 1, and C, lanes 1 and 3). The molecular mass of the ~18-kDa MBD4 moiety is consistent with the predicted size of the putative 175-aa SF. It should be noted that the intensity of the ~18-kDa MBD4 polypeptide is weak relative to that of the FL form. However, this may

not limit functionality, since extremely low levels of UNG are sufficient for efficient CSR (13). Together, our findings indicate that a unique MBD4 isoform spanning the C-terminal DNA glycosylase domain is expressed in activated splenic B cells and the CH12 cell line.

Variant MBD4 expression is retained in *Mbd4*$^{\Delta 2\text{-}5/\Delta 2\text{-}5}$ mice. Our earlier studies showed that *Mbd4*-deficient mice lacking exons 2 to 5 (16), referred to here as *Mbd4*$^{\Delta 2\text{-}5/\Delta 2\text{-}5}$ mice, supported efficient CSR (17). However, the *Mbd4*$^{\Delta 2\text{-}5/\Delta 2\text{-}5}$ locus retains the puromycin resistance gene and the phosphoglycerate kinase (PGK) promoter, which could support the transcription of the residual 3′ exons (16). Although Western blot assays indicate that activated splenic *Mbd4*$^{\Delta 2\text{-}5/\Delta 2\text{-}5}$ B cells fail to express FL MBD4, they actively express an ~18-kDa MBD4 polypeptide (Fig. 1B, compare lane 1 with lanes 2 to 4). The complexity of the *Mbd4*$^{\Delta 2\text{-}5/\Delta 2\text{-}5}$ locus prompted us to construct a new *Mbd4* KO in which the DNA glycosylase domain is completely deleted.

Targeted deletion of *Mbd4* exons 6 to 8 in CH12 cells. We used gene-targeted homologous recombination in a CH12 subclone, C.24, to replace exons 6 to 8 and the 3′ UTR of the *Mbd4* gene with a neomycin resistance gene (*neo*^{r}) and a negative selection thymidine kinase (TK) cassette (see Fig. S4A in the supplemental material). The CH12 cell line can be induced to undergo IgA switching (25) and has been used for targeted gene deletion (26–30). The 5′ and 3′ *Mbd4* homology arms, of 2.85 and 5.34 kb, respectively, were cloned into the targeting vector pLNTK. After gene targeting, the *neo*^{r} gene, flanked by 34-bp *loxP* sequences (31), was deleted by exposure to Cre recombinase. Gene deletions were confirmed by Southern blot analyses with two independent probes (Fig. S4B). For the endogenous allele, 7.35- and 7.7-kb BamH1 restriction fragments are found by analysis with the 5′ and 3′ probes, respectively. In contrast, 6.0- and 6.9-kb fragments appear upon examination of the targeted allele using the same probes (Fig. S4A and B). Cre-mediated deletion results in removal of the *neo*^{r} gene, along with a BamH1 site, leaving a single *loxP* sequence at the site. Following deletion by Cre, the 6.0- and 6.9-kb fragments become a single 11-kb fragment that can be analyzed with either probe (Fig. S4A and B).

We identified two clones, M19$^{N/+}$ and 1A-12$^{N/+}$, in which the targeting construct was integrated into one allele, which was then subjected to Cre recombinase to create *neo*^{s} clones M19$^{\Delta/+}$ and 1A-12$^{\Delta/+}$, respectively (Fig. S4B). The 1A-12$^{\Delta/+}$ clone was targeted on the second allele and was exposed to Cre recombinase to create 1A-12$^{\Delta/\Delta}$, referred to as *Mbd4* KO (Fig. S4B). A full pedigree of C.24 derivative clones and subclones used in our studies is provided in Fig. S1A in the supplemental material. Next, *Mbd4* transcript and protein levels were examined in control and *Mbd4*-deleted cells that were either left unstimulated or activated with CIT to induce $\mu \rightarrow \alpha$ CSR. Quantitative reverse transcription-PCR (qRT-PCR) using primers for exon 6 and the 3′ UTR demonstrates that the *Mbd4* transcript is induced by CIT in control cells but not in KO cells (Fig. 1D). Western blot assays show that FL and SF MBD4 polypeptides are absent in 1A-12$^{\Delta/\Delta}$ cells relative to controls (Fig. 1C, compare lanes 1 and 3 with lanes 2 and 4). Thus, MBD4 expression is completely abolished in 1A-12$^{\Delta/\Delta}$ cells. Furthermore, MBD4 protein levels are dependent on the number of intact alleles, since the level of FL MBD4 expression in 1A-12$^{\Delta/+}$ cells is about half that found in control cells by Western blot analyses (Fig. 1E).

***Mbd4* deficiency in CH12 cells is associated with reduced IgA switching.** To determine whether *Mbd4* mediates CSR, we analyzed control and *Mbd4* KO cells for $\mu \rightarrow \alpha$ switching following activation with CIT for 24 h. Relative to that in controls, the level of IgA switching is reduced approximately 4-fold ($P < 0.01$) in 1A-12$^{\Delta/\Delta}$ cells and 2-fold ($P < 0.01$) in heterozygous M19$^{N/+}$, 1A-12$^{N/+}$, and 1A-12$^{\Delta/+}$ cells, indicating *Mbd4* haploinsufficiency (Fig. 2A). The CSR frequencies associated with subclones derived from 1A-12$^{\Delta/+}$ and 1A-12$^{\Delta/\Delta}$ cells recapitulate the $\mu \rightarrow \alpha$ CSR frequencies of their parental clones, 1A-12$^{N/+}$ and 1A-12$^{N/\Delta}$ (Fig. S1 in the supplemental material). Accordingly, the haploinsufficiency of 1A-12$^{\Delta/+}$ cells for IgA switching is reflected by

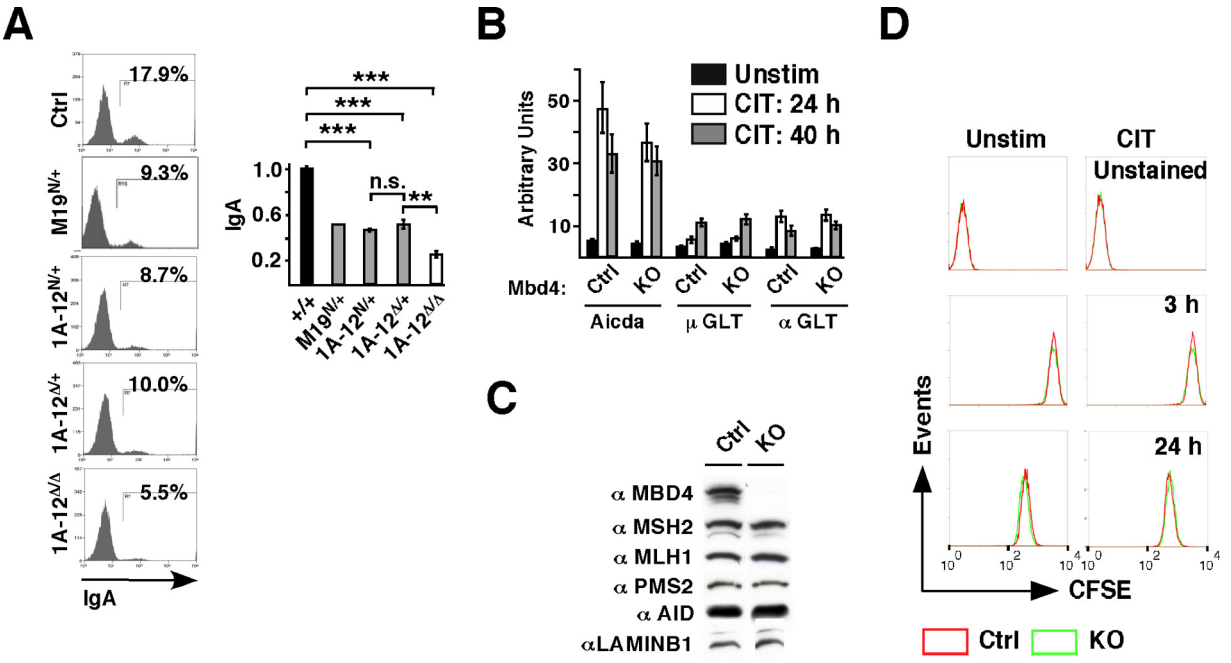

FIG 2 CSR is impaired in *Mbd4* KO cells. Control (Ctrl) CH12 cells and *Mbd4*-deficient cells were treated with CIT for 24 h (A, C, and D) or as indicated (B). (A) Ctrl (+/+), *Mbd4* HET (1A-12$^{N/+}$, 1A-12$^{\Delta/+}$, M19$^{N/+}$), and KO (1A-12$^{\Delta/\Delta}$) cells were analyzed by FACS for IgA expression. The *Mbd4* targeted allele with (N) and without (Δ) the *neo*^{r} cassette is shown. Representative FACS analyses (left) and average percentage of IgA^{+} cells after CSR with SEMs from two to four independent experiments (except for M19$^{N/+}$ [$n = 1$]) (right) are shown. Asterisks indicate significant differences by Student's two-tailed *t* test (*, $P < 0.05$; **, $P < 0.01$; ***, $P < 0.001$). n.s., not significant. (B) Aicda (AID) and GLTs μ and α were analyzed by qRT-PCR, and results were normalized to those for 18S rRNA. Averages with SEMs from two samples and two independent experiments are shown. Unstim, unstimulated. (C) Western blot analysis of nuclear extracts from Ctrl and *Mbd4* KO (1A-12$^{\Delta/\Delta}$) cells using the indicated Abs. The blot shown is representative of two independent experiments. (D) Proliferation was monitored by CFSE dilution over time in unstimulated or CIT-treated Ctrl (red) and Mbd4 KO (green) cells that were either left unstained or CFSE loaded (15 μM) and analyzed by FACS at 3 and 24 h postloading. Results shown are representative of three independent experiments.

the half-dose of FL MBD4 expression relative to expression in control and 1A-12$^{\Delta/\Delta}$ cells in Western blot studies (Fig. 1E and 2A).

To ensure that *Mbd4* KO has no collateral effects on other mediators of CSR, we analyzed germ line transcripts (GLTs) and AID expression by qRT-PCR. Germ line transcription initiates at a TSS upstream of an I exon, proceeds through the S region, and terminates downstream of the corresponding C_H gene. The reduction in the frequency of CSR in *Mbd4* KO cells was not accompanied by any detectable alteration in steady-state μ and α GLTs, or in *Aicda* (AID) mRNA expression, following CIT treatment (Fig. 2B). Western blot analyses indicate that AID levels in KO cells were comparable to those found in control cells (Fig. 2C). Because CSR is linked to cell division (32), we examined cellular proliferation in control and *Mbd4*-deficient cells by carboxyfluorescein succinimidyl ester (CFSE) dilution. Cells that were left unstimulated and those that were treated with CIT showed similar levels of uptake of CFSE and equivalent dilutions 24 h later, indicating that cell proliferation is unperturbed by *Mbd4* deficiency (Fig. 2D).

MMR heterodimers MSH2/MSH6 and MLH1/PMS2 are required for efficient CSR (6). Diminished levels of MMR proteins are found in activated splenic B cells and murine embryonic fibroblasts (MEF) from *Mbd4*$^{\Delta 2\text{-}5/\Delta 2\text{-}5}$ mice (16, 17). Western blot analyses indicate that MLH1, PMS2, and MSH2 levels are unchanged in CIT-activated control and *Mbd4* KO cells (Fig. 2C). Global gene expression analyses identified only 18 of 3×10^4 genes with at least a 2-fold expression change in *Mbd4* KO cells relative to controls (GEO accession no. GSE51559). These gene expression differences are likely to reflect normal differences between cell clones. We conclude that studies focused on 1A-12$^{\Delta/+}$ and 1A-12$^{\Delta/\Delta}$ are representative of the CSR potential for these genotypes. Hence, the CSR deficit in *Mbd4* KO cells cannot be ascribed to perturbation of GLTs, AID, cell proliferation, MMR protein levels, or global gene expression.

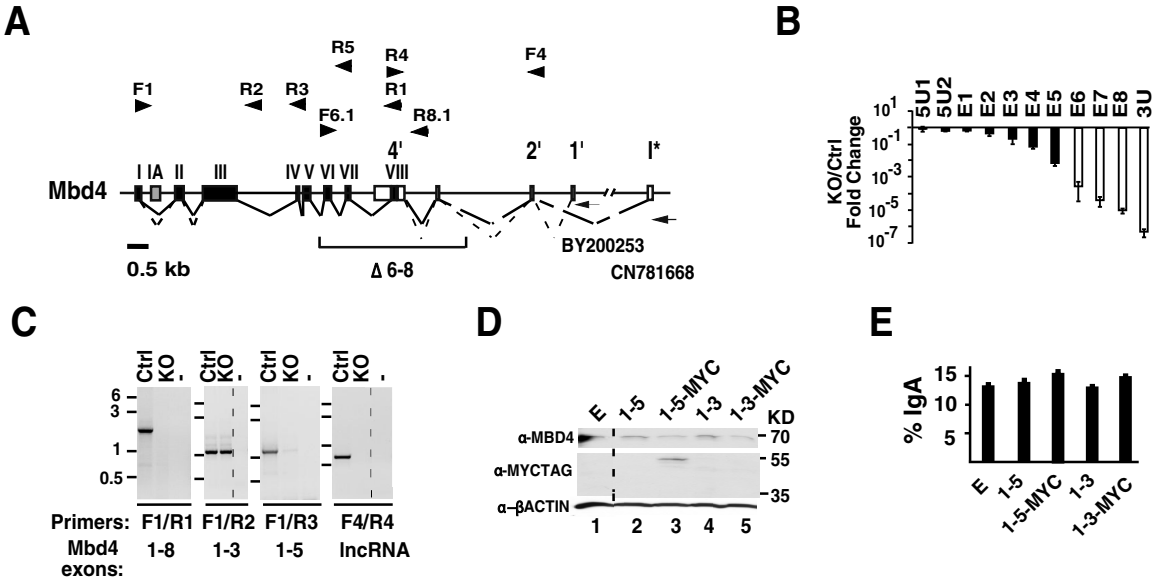

FIG 3 Expression of truncated MBD4 has no deleterious effects on CSR. (A) Diagram of the *Mbd4* locus (chromosome 6, coordinates 115840698 to 115853371 [mm9]) with a partial representation of the antisense lncRNAs (NCBI Nucleotide database accession no. CN781668 and BY200253). Splicing of *Mbd4* mRNA produces *Mbd4* exons 1 to 8 (XM_006505679.2) (solid line) or *Mbd4* exons 1 to 3 (AK148171) (dashed line). Splicing of lncRNA exons 1* to 4′ and 1′ to 4′ (open rectangles) produces lncRNA1 (CN781668) (long dashed lines) and lncRNA2 (BY200253) (short dashed lines). PCR primers (arrowheads) are indicated. (B to E) Control (Ctrl) and *Mbd4* KO (1A-12$^{\Delta/\Delta}$) cells were activated with CIT for 24 h. (B) *Mbd4* gene expression in control and *Mbd4* KO cells was examined using Affymetrix mouse genome 1.0 ST arrays (GEO accession no. GSE51559). Microarray probes hybridizing to the 5′ UTR (5U1 and 5U2), exons 1 to 5 (E1 to E5) (filled bars), exons 6 to 8 (E6 to E8), and the 3′ UTR (3U) (open bars) are indicated. (C) RT-PCR using control and *Mbd4* KO cDNA templates and primer F1 in combination with primer R1, R2, or R3 detects *Mbd4* exons 1 to 8, 1 to 3, or 1 to 5, respectively. Primers F4 and R4 detect lncRNAs. (D and E) Control cells were stably transfected with empty (E), MBD4 exon 1 to 5 (1-5), C-terminally MYC-tagged MBD4 exon 1 to 5 (1-5-MYC), MBD4 exon 1 to 3 (1-3), or C-terminally MYC-tagged MBD4 exon 1 to 3 (1-3-MYC) constructs. (D) Western blot analyses of nuclear extracts from stably transfected CH12 cells using anti-MBD4 or antiactin Abs. Results representative of two independent analyses are shown. (E) Average IgA switching frequencies from FACS analyses with SEMs ($n = 4$).

Truncated *Mbd4* proteins lack dominant negative effects. Because truncated MBD4 protein arising from residual expression of exons 1 to 3 or exons 1 to 5 could potentially act as dominant negative mutants (33) and inhibit CSR, we analyzed the pattern of Mbd4 transcription in control and *Mbd4* KO cells. Although microarray analyses indicate that the transcript abundance of *Mbd4* exons 1 to 3 is invariant, longer transcripts are severely reduced, beginning at exon 4, for the *Mbd4* KO relative to controls (Fig. 3A and B). These findings were confirmed using conventional RT-PCR on samples prepared by rapid amplification of 3′ cDNA ends (3′ RACE) to verify the presence of polyadenylation (Fig. 3C). Transcripts encompassing *Mbd4* exons 1 to 5 are evident in controls but are essentially undetectable in KO cells, in agreement with the microarray data (Fig. 3B and C). Finally, the long noncoding RNAs (lncRNAs) (NCBI Nucleotide database no. CN781668 and BY200253) that overlap the *Mbd4* 3′ UTR in the antisense direction are absent in *Mbd4* KO cells (Fig. 3C). Hence, no spurious transcripts originating from the 5′ end of the gene are detected in *Mbd4* KO cells.

To test for potential dominant negative effects, MBD4 was tagged with a MYC epitope at the C terminus, enabling assessment by Western blot assays. Ectopic expression of protein from MBD4 exons 1 to 5 but not from exons 1 to 3 could be confirmed in stable transfectants derived from control CH12 cells that also express endogenous FL *Mbd4* (Fig. 3D). Stable expression of *Mbd4* exons 1 to 5 had no effect on IgA switching following induction with CIT (Fig. 3E). Thus, potential *Mbd4* transcripts originating from the 5′ end of the gene do not confer dominant negative effects on CSR. We conclude that the reduced CSR frequency in *Mbd4* KO cells is most likely due to targeted deletion spanning the region from exon 6 to the 3′ UTR. Collectively, our findings indicate that both *Mbd4* FL and SF transcripts and polypeptides are essentially ablated in *Mbd4* KO cells.

Impaired CSR following CRISPR-Cas9 ablation of *Mbd4* gene expression. To independently query the dependency of CSR on *Mbd4* expression, we employed the clustered regularly interspersed short palindromic repeat (CRISPR) genome-editing tool to disrupt *Mbd4* expression in CH12 cells (34, 35). Using the mammalian-codon-optimized Cas9 nuclease and a guide RNA (gRNA) targeting the *Mbd4* exon 8 splice acceptor, we generated a 299-bp homozygous deletion spanning all of exon 8 and a portion of the 3′ UTR in a clone, AS23 (Fig. 4A and B). We systematically evaluated the expression of the *Mbd4* transcript in control and A23 cells. The CRISPR-generated deletion caused destabilization of the *Mbd4* transcript; expression was abolished in both unstimulated and CIT-induced AS23 cells relative to controls, as determined by qRT-PCR assays using primers for exon 6 and the 3′ UTR (Fig. 4C). The steady-state levels of *Mbd4* transcripts spanning exons 1 to 5 and exons 1 to 7 were severely reduced for AS23 cells relative to control cells (Fig. 4D). In contrast, expression of *Mbd4* exons 1 to 3 was detected in both control and AS23 cells (Fig. 4D). Hence, the mRNA transcripts for FL and SF MBD4 protein are abolished in AS23 cells. Accordingly, the level of IgA switching is reduced 2.7-fold ($P < 0.0001$) following CIT treatment in AS23 cells relative to controls (Fig. 4E). We conclude that the reduced CSR in AS23 cells is related to *Mbd4* deficiency, since there was no change in the expression of GLTs μ and α, or of AID transcripts, relative to that in controls (Fig. 4F).

Ectopic expression of *Mbd4* rescues CSR. Complementation studies were performed to determine whether CSR can be rescued in *Mbd4*-deficient cell lines. MBD4 has two well-defined functions associated with the C terminus spanning exons 5 to 8: (i) a uracil DNA glycosylase activity (21) and (ii) a capability for interaction with MLH1 (36). The Y514 residue located in exon 7 resides within the catalytic core, and a Y514F substitution renders the glycosylase inactive (15, 21). The Y514 residue is outside the MBD4–MLH1 interaction region, based on the analogous human MBD4–MLH1 interaction site (36). Transient transduction of FL *Mbd4*^{WT} in control cells followed by CIT activation led to diminished cell viability relative to that of an empty construct, indicating that *Mbd4* FL expression was toxic to the cells (see Fig. S5 in the supplemental material). Cell death was not a result of the transduction process or construct size, as evidenced by the fact that cells stably transduced with an *Mbd4*-flipped (nonexpressed) construct were viable over time (Fig. S5B and C). However, we found that truncated MBD4 spanning exons 4 to 8 (M$^{4\text{-}8}$) was not toxic when ectopically expressed. We selected stable transfectants expressing M$^{4\text{-}8}$, M$^{4\text{-}8Y514F}$, and empty constructs in AS23 and *Mbd4* KO cells. Western blot analyses confirmed that M$^{4\text{-}8}$ is stably expressed prior to and following CIT activation and that the expression levels of M$^{4\text{-}8}$ and M$^{4\text{-}8Y514F}$ are equivalent (Fig. 4G). CSR deficiency was rescued in AS23 cells ($\sim$1.5-fold [$P < 0.0001$]) by M$^{4\text{-}8}$ expression relative to the empty construct and the catalytically inactive M$^{4\text{-}8Y514F}$ construct (Fig. 4H). The statistically significant, albeit modest, CSR rescue may be due to the use of the truncated MBD4, which is not optimal for this purpose. We conclude that the CSR defect in the *Mbd4* KO cell lines is not a consequence of off-target effects; rather, it is related to *Mbd4* deficiency.

***Mbd4* deficiency impairs Sμ region DSB formation.** S region-specific DSBs are obligatory intermediates of the CSR reaction (8, 10, 37). DSBs in S regions are formed by AID-induced deamination of dC to U and the removal of U by UNG to form an abasic site, followed by breakage of the phosphate backbone by APEs (Fig. 5A) (38, 39). U-G mismatches generated by AID are also substrates for MMR (Fig. 5B) (6, 40). DSBs are focused to the Sμ tandem repeats (TRs) that compose the Sμ core sequences replete with AID hot spot motifs and, less frequently, to 5′ Sμ, which contains fewer TRs (41). When dC residues are closely positioned on complementary strands, AID-initiated staggered DSBs are created (Fig. 5Ac). Blunt DSBs are produced from staggered breaks when the overhanging nucleotide is removed by an exonuclease (Fig. 5Ad). When AID-induced deamination events are far apart, S region DSBs are formed by the combined action of the BER and MMR pathways (Fig. 5B). The interaction of MBD4 with

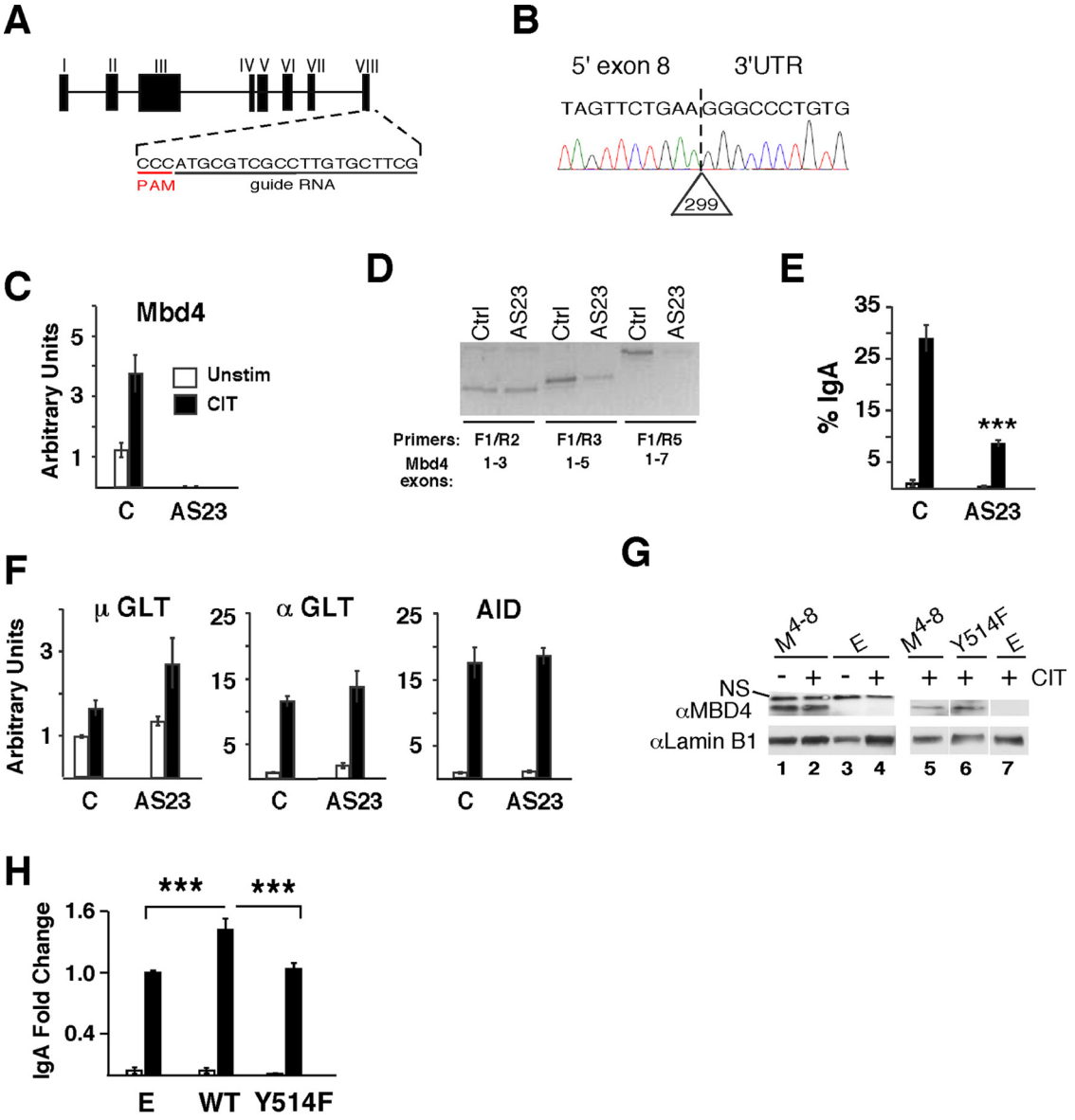

FIG 4 Complementation of impaired CSR in *Mbd4*-deficient cell lines. (A) The gRNA with protospacer adjacent motif (PAM) used to target *Mbd4* by CRISPR-Cas9 is aligned to the genomic map of the *Mbd4* gene exons (rectangles) and introns (lines). (B) The gRNA and Cas9 nuclease were transfected into CH12 control cells, and AS23 was isolated. The sequencing chromatogram of the AS23 clone depicts a homozygous 299-bp deletion spanning *Mbd4* exon 8 and extending into the 3′ UTR. (C to H) CH12 control (Ctrl) and AS23 cells were either left unstimulated or treated with CIT for 20 h. (C) qRT-PCR was performed using cDNA from control and AS23 cells and primers F6 and R1 (Fig. 3A). (D) RT-PCR using control and AS23 cDNA and primer F1 in combination with primer R2, R3, or R5 detects *Mbd4* exons 1 to 3, *Mbd4* exons 1 to 5, or *Mbd4* exons 1 to 7, respectively (Fig. 3A). (E) Proportions of control and AS23 cells expressing surface IgA. Averages and SEMs from two to four independent experiments are shown. Asterisks indicate significant differences by Student's two-tailed *t* test (***, $P < 0.001$). (F) Transcript levels for AID and for GLTs μ and α were analyzed by qRT-PCR and were normalized to those for 18S rRNA. Averages with SEMs from at least two samples and two independent experiments are shown. (G and H) Pools of AS23 cells stably expressing empty (E), MBD4$^{4-8}$ (M$^{4-8}$), and *Mbd4*$^{4-8Y514F}$ (Y514F) constructs were analyzed. Stable transfectants were either left unstimulated or treated with CIT, as indicated. (G) Western blot assays using an anti-MBD4 or anti-lamin B1 Ab and stable AS23 transfectants. (H) Stable AS23 transfectants were analyzed for IgA surface expression by FACS analyses. Averages with SEMs from at least two samples and two independent experiments are shown.

MLH1 and PMS2 *in vivo* (17, 36) implies that *Mbd4* deficiency might impact MMR-dependent DSB formation.

Using ligation-mediated PCR (LM-PCR) to measure Sμ DSB abundance, we examined the incidence of Sμ DNA breaks in *Mbd4* KO and control cells. We focused on the prevalent Sμ DSBs and not on the less frequent DSBs in downstream S regions (10). Technical difficulties precluded analysis of staggered DNA ends via T4 DNA polymerase

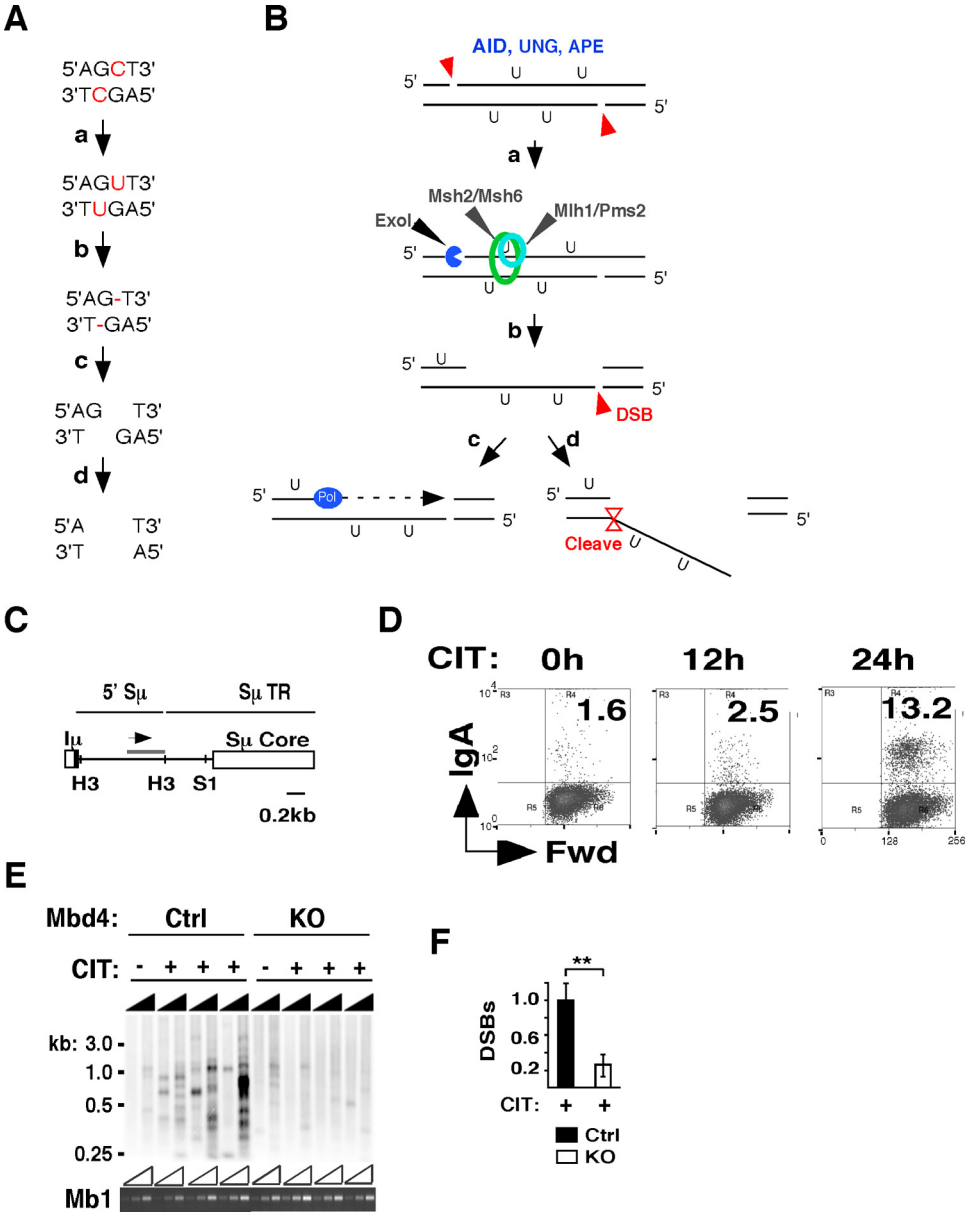

FIG 5 Sμ DSB formation is reduced in *Mbd4*-deficient cells. (A) Diagrammatic summary of AID- and BER-induced DSB formation. (a) AID deaminates dC to produce uracil (U) residues. An AID hot spot motif (DGYW/WRCH [D stands for G, A, or T; H stands for C, T, or A]) is shown. (b) UNG acts on U residues to produce abasic sites. (c) AP endonucleases sever the phosphate backbone to form staggered DSBs. (d) Nucleases polish overhangs to form blunt DSBs that are substrates in the LM-PCR. (B) The BER pathway creates SSBs. MutSα (MSH2/MSH6) and MutLα (MLH1/PMS2) accumulate at U-G mismatches and attract Exol to an adjacent nick. Exol excises sequence between nicks on opposite strands to generate a DSB. The gap can be filled in by a translesion polymerase, or the overhang can be removed by a 5′ flap endonuclease (6). (C) Schematic showing the HindIII (H3) and SacI (S1) sites, the LM-PCR locus-specific forward primer (arrow), and the Sμ probe (horizontal shaded bar), relative to Iμ, 5′ Sμ, Sμ TRs, and Sμ core TR elements. (D) FACS analyses of forward scatter and surface IgA on CH12 control cells at 0, 12, and 24 h following CIT activation. (E) LM-PCR products were derived from control (Ctrl) and *Mbd4* KO cells that were either left untreated or induced with CIT for 12 h and were then analyzed by Southern blotting using the Sμ probe. Southern blots were quantified using ImageQuant software. A representative Southern blot shows 5-fold serial dilutions of Sμ-specific LM-PCR products (filled triangles). Semiquantitative PCR amplification of the Mb1 gene (29, 31, and 33 cycles) (open triangles) was used as a loading control. (F) Relative levels of DSB induction in control and *Mbd4* KO cells. Data are averages from three independent samples and SEMs. The result for the control is set to 1. Asterisks indicate significant differences by Student's two-tailed *t* test (**, $P < 0.01$).

end polishing (42). In the LM-PCR assay, an asymmetric, double-stranded oligonucleotide linker is ligated to blunt DSBs, and ligated products are amplified using a locus-specific 5′ Sμ primer paired with a 3′ linker primer and are analyzed by Southern hybridization (Fig. 5C) (10, 37). We examined Sμ DSB formation in cells that were either

left untreated or activated by CIT for 12 h, a time point before substantial CSR, as indicated by fluorescence-activated cell sorter (FACS) analyses for surface IgA (Fig. 5D). Semiquantitative PCR amplification of the Mb1 gene served as a loading control (Fig. 5E). Few DNA breaks were detected in unstimulated control or *Mbd4* KO cells (Fig. 5E). In contrast, following CIT treatment, DSBs were significantly induced in controls but not in MBD4 KO cells ($P < 0.01$) as determined by quantification of the Southern blot data (Fig. 5F). Our studies indicate that *Mbd4* contributes significantly to CSR through the genesis of Sμ DSBs.

***Mbd4* deficiency alters the location and quality of Sμ DSBs.** AID targeting to a DNA substrate is context dependent and appears to be dictated, at least in part, by the S region primary sequence (43, 44). We analyzed the DNA sequences at Sμ DSBs from normal splenic B cells and compared them to those from CH12 cells as an independent test of their physiological relevance. In WT, *Msh2*-deficient, and *Mlh1*-deficient B cells, many Sμ DSBs (41%) localized to AID hot spot motifs WRC/GYW (where W stands for A or T, R stands for G or A, and Y stands for C or T) (8, 10) (Fig. 6A). In contrast, residual DSBs in AID- or Ung-deficient B cells failed to localize in AID consensus motifs, indicating the specificity of AID or UNG in this reaction (10) (Fig. 6A). We cloned LM-PCR DSB products from CH12 control and *Mbd4* KO cells and found that 43% and 53% localized to AID hot spots, respectively, thereby establishing CH12 and *Mbd4* KO cells as models for DSB formation analyses (Fig. 6A). We conclude that the reduction in the level of Sμ DSB formation in *Mbd4* KO cells appears to be unrelated to a lapse of AID and UNG function.

Sμ/Sx (where Sx is a downstream switch region) recombination crossover points occur preferentially in Sμ TRs and less commonly in 5′ Sμ, reflecting the distribution of AID hot spot motifs across the S region (45). Sμ DSBs derived from WT splenic B cells locate predominantly (77%) at Sμ TRs rather than in the 5′ Sμ region (23%) (8, 10) (Fig. 6B, left). Although Sμ DSBs from CH12 control cells focus more on Sμ TRs (59%) than on 5′ Sμ (39%), *Mbd4* KO cell-derived DSBs localize preferentially to Sμ TRs (82% [$P < 0.05$]) with an increased focus on AID hot spots ($P < 0.05$) relative to that for controls (Fig. 6B, right). This DSB distribution parallels that found in Msh2-deficient B cells, which also localize preferentially to Sμ TRs ($P < 0.05$) and away from the 5′ Sμ region (Fig. 6B, left) (46). These findings are consistent with the hypothesis that *Mbd4* function in the genesis of DSBs is linked with the MMR pathway.

In Sμ DNA, AGCT, GGCT, and TGCT (listed in order of frequency of occurrence) are common iterations of an extended AID consensus hot spot motif, DGYW/WRCH (where D stands for G, A, or T, H stands for C, T, or A, R stands for G or A, and W stands for A or T). However, DGYW only partially accounts (~40%) for the Sμ DSB sequence distribution. We simplified the DSB analysis and asked whether there was a preference for nearest-neighbor nucleotides adjacent to the G-C breakpoint. Although DSBs were evenly distributed among AG, TG, and GG in CH12 control cells and WT splenic B cells, breaks localized more to AG in *Mbd4* KO cells than in controls (47.4% versus 27.8% [$P < 0.01$]) (Fig. 6C and D). Enrichment of AG breaks was also found in *Msh2*-deficient (47.1% versus 25.7% [$P < 0.05$]) and *Mlh1*-deficient B cells relative to WT B cells (Fig. 6C, right and inset). We conclude that *Mbd4*, like *Msh2*, is required for the diversification of DSB location and motif usage within S regions, which may indicate a shared mechanism for generating and processing DSBs.

Sμ-Sα joining is altered in *Mbd4* KO cells. Sμ-Sα switch junction quality reflects the resolution of S region DSBs and is determined in part by the integrity of the MMR pathways in which *Mlh1* or *Pms2* deficiency produces an increase in junctional microhomology (47). Junctional microhomology is observed when the precise location of the recombination breakpoints cannot be mapped because the Sμ and Sx germ line sequences are identical at the junction (Fig. 7A). Typically, S-S junctions have 0 to 3 bp of microhomology between the Sμ donor region and the downstream Sx acceptor region, whereas microhomology of >4 bp is rare (48). We cloned and sequenced Sμ-Sα junctions from control and *Mbd4* KO cells stimulated with CIT for 24 h (see Fig. S6 and

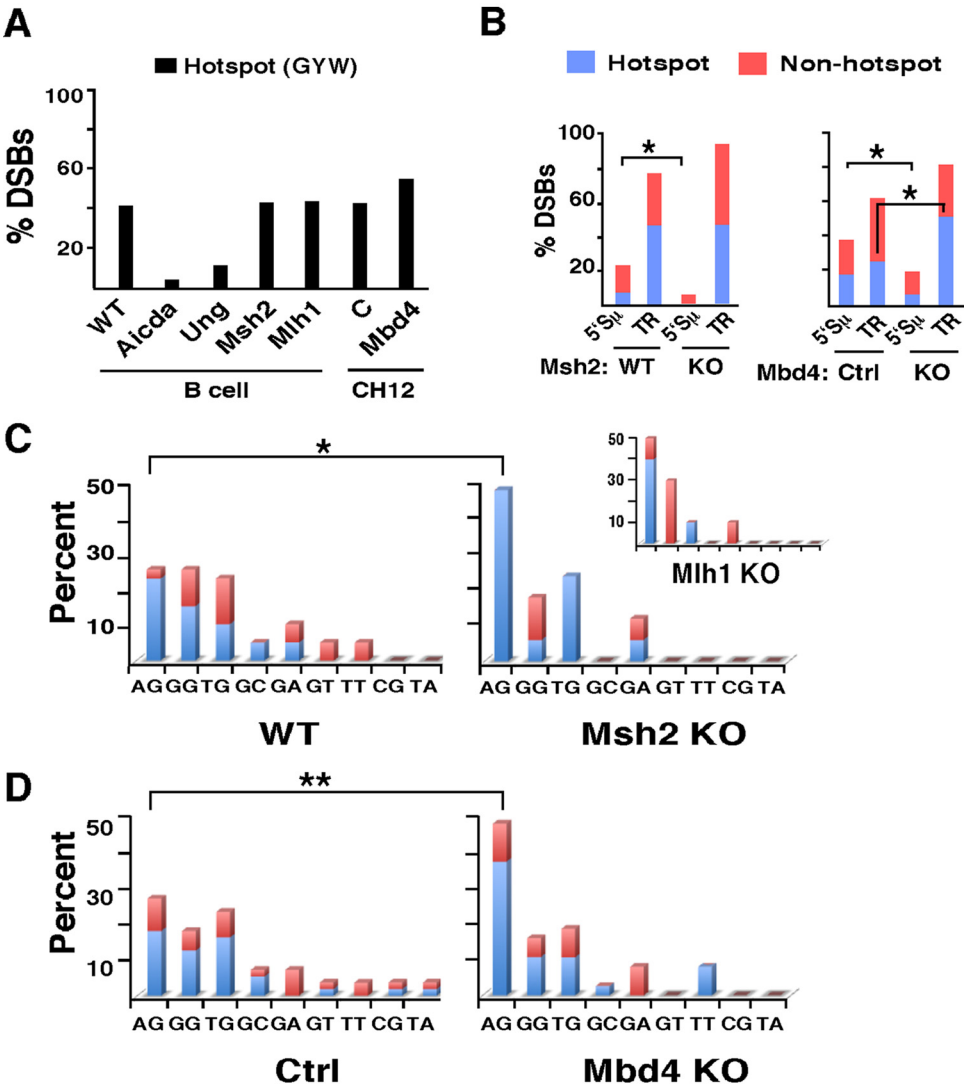

FIG 6 Similar DSB distributions in *Mbd4* KO and *Msh2*-deficient B cells. CH12 control (Ctrl) and *Mbd4* KO cells were treated with CIT for 12 h and were then analyzed by LM-PCR. Control ($n = 52$) and *Mbd4* KO ($n = 39$) LM-PCR products were subjected to DNA sequence analysis to assess DSB sites. DNA sequences surrounding DSBs from WT B cells ($n = 135$) and from B cells deficient in AID ($n = 26$), Ung ($n = 17$), *Msh2* ($n = 30$), or *Mlh1* ($n = 16$) have been described previously (8, 10). *P* values are from χ^2 analyses (*, $P < 0.05$; **, $P < 0.01$). (A) DSBs occurring at GYW/WRC AID hot spot motifs. C, control. (B to D) DSB sites located at extended AID hot spots, defined as DGYW/WRCH, were assessed. DSBs derived from WT B cells ($n = 39$) or from B cells deficient in *Msh2* ($n = 17$) or *Mlh1* ($n = 10$), activated with LPS plus IL-4 for 48 h (8, 10), or DSBs from CH12 control ($n = 54$) and *Mbd4* KO ($n = 38$) cells were analyzed. (B) Proportion of DSBs located at 5′ Sμ or in Sμ TRs and their localization to the AID hot spot motif or non-hot spots. (C and D) Characterization of the DSBs by nearest-neighbor analysis using the format NX (where X indicates the nucleotide at which the break occurred and N is the 5′ neighboring nucleotide) with their localization to AID hot spot (blue) or non-hot spot (red) motifs. The percentage of breaks detected at each dinucleotide is shown.

S7 in the supplemental material). In agreement with previous studies (48), the majority (88.2%) of Sμ-Sα junctions from control cells ($n = 34$) had microhomology between 0 and 3 nucleotides, while a minority (11.8%) displayed microhomology of 4 nucleotides or more (Fig. 7A and B). The Sμ-Sα junctions from *Mbd4* KO cells ($n = 24$) were markedly different from those in control cells. The proportion of direct joins was diminished in *Mbd4* KO cells from that in controls (12% versus 29.4% [$P < 0.05$]), while the proportion of joins with 4 or more nucleotides increased (29.2% versus 11.8% [$P < 0.05$]) (Fig. 7B). Overall, the average microhomology length increased from 1.91 nucleotides for controls to 2.82 nucleotides for *Mbd4* KO cells, and this difference is significant (*P*, 0.046 by the Mann-Whitney test) (Fig. 7C). The increased microhomology

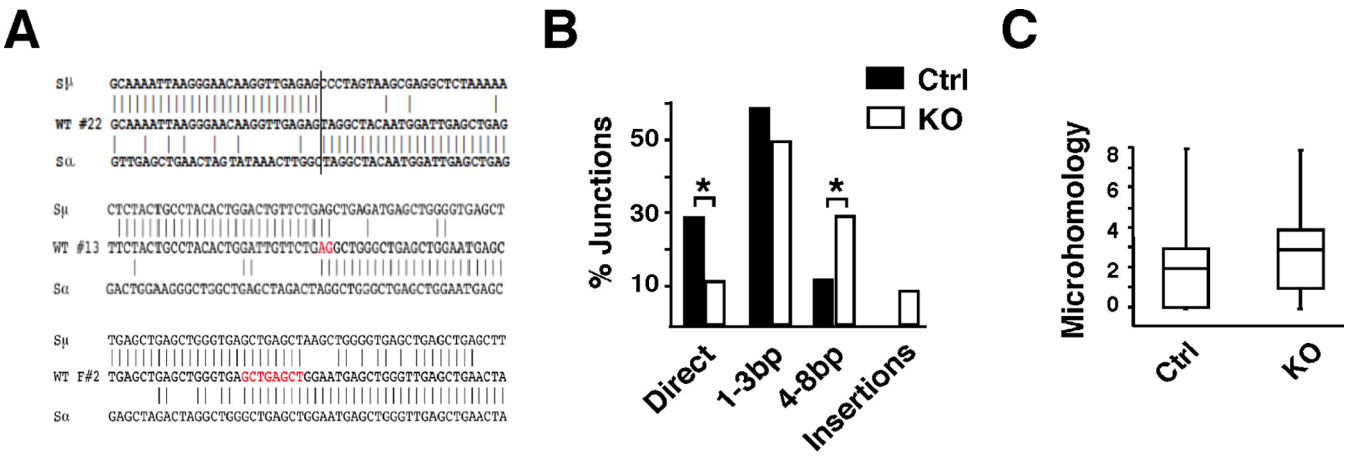

FIG 7 Increased microhomology in Sμ-Sα junctions from *Mbd4* KO cells. Sμ-Sα junctions were amplified from genomic DNA prepared from CH12 control (Ctrl) ($n = 34$) and *Mbd4* KO ($n = 24$) cells stimulated with CIT for 24 h, and the DNA sequences were derived (Fig. S6 and S7). (A) Representative examples of Sμ-Sα junctions in control cells with blunt, 2-base overlap, and 8-base microhomologies (red letters). (B) Percentages of Sμ-Sα junctions with the indicated nucleotide overlaps or insertions. Chi-square analysis was used to determine *P* values (*, $P < 0.05$). (C) Mann-Whitney analysis of a box-and-whisker plot comparing the proportions of Sμ-Sα junctions displaying microhomology from CH12 control and *Mbd4* KO cells.

at Sμ-Sα junctions in *Mbd4* KO cells is similar to that found for *Mlh1*-deficient cells (47) and implies that *Mbd4* contributes to efficient repair of DSBs into direct joins.

DISCUSSION

In this report, we identify a role for *Mbd4* in CSR and the formation of S region-specific DSBs. Induction of *Mbd4*-deficient B cell lines constructed using both classical targeted homologous recombination and CRISPR methods led to 80% reduced CSR frequency. Complementation studies revealed that ectopic expression of FL MBD4 caused cellular toxicity. Several lines of evidence have implicated MBD4 in apoptotic control or signaling (49). MBD4 has been shown to interact directly with proapoptotic Fas-associated death domain protein (FADD) in a complex with MLH1 (50). MBD4 was also found to bind MLH1 and DNA methyltransferase 1 (DNMT1) in *Xenopus* embryos (51). Depletion of MBD4 or MLH1 increased the survival of DNMT1-depleted *Xenopus* embryos, while overexpression induced apoptosis (51). These studies provide a plausible explanation for B cell death upon exposure to ectopically expressed FL MBD4. We circumvented this issue by expressing MBD4 exons 4 to 8. Although truncated MBD4 rescued CSR, the Y514F substitution that renders the MBD4 uracil DNA glycosylase inactive (15, 21) failed to support CSR. The Y514 residue is outside the MBD4–MLH1 interaction region (based on the analogous human MBD4–MLH1 interaction site [36]) and is unlikely to interfere with these interactions. Collectively, our studies suggest that MBD4 function in CSR requires the *Mbd4* uracil DNA glycosylase activity.

Analysis of MBD4 protein in CH12 and B cells revealed the expression of FL and SF isoforms. We considered the intriguing possibility that SF MBD4 is functionally required for efficient CSR while the FL MBD4 is dispensable. First, in *Mbd4*$^{\Delta 2\text{-}5/\Delta 2\text{-}5}$ B cells, some version of the SF MBD4 was expressed and CSR was intact. Second, when expression of both the FL and SF MBD4 isoforms was abolished (measured at the transcript and protein levels), CSR was diminished in our *Mbd4*-deficient cell lines. FL MBD4 carries the MBD, which may be crucial for DNA demethylation and dispensable for CSR. Finally, our complementation studies indicated that MBD4 exons 4 to 8 were sufficient to support CSR, albeit modestly. Further studies are necessary to determine the relative contributions of FL MBD4 and SF MBD4 to CSR.

During CSR, S region DSBs are obligate intermediates that result from the removal of uracil introduced by AID deamination. Our analyses of Sμ DSBs in *Mbd4*-deficient cells revealed striking similarities to those detected in MMR-deficient B cells. First, *Msh2*- and *Mlh1*-deficient B cells (8) and *Mbd4*-deficient cell lines all had fewer Sμ DSBs than their WT cell counterparts upon CSR activation. Second, rare Sμ DSBs from *Msh2*-

deficient B cells accumulated in Sμ TRs and were underrepresented in the 5′Sμ region. *Mbd4* deficiency led to a similarly perturbed distribution of Sμ DSBs. Finally, Sμ DSBs from *Mbd4*- or *Msh2*-deficient cells displayed increased localization to AID hot spots and increased homogeneity of the breakpoint sequence in nearest-neighbor analyses. AID hot spot motifs densely populate the Sμ TRs, whereas these motifs are sparsely represented in the 5′ Sμ region. It has been proposed that when distantly spaced uracil residues undergo single-strand scission via BER, long DNA overhangs are produced and are then processed to yield DSBs (6) (Fig. 5B). By this logic, long DNA overhangs are more likely to occur in the 5′ Sμ region, where uracil residues are far apart due to the relative paucity of AID hot spot motifs than they are in the TRs. Thus, in *Mbd4*- and MMR-deficient cells, the 5′ Sμ region is underutilized as a site for DSB formation, presumably because the processing of long DNA overhangs into DSBs is impaired. Collectively, our DSB formation findings raise the intriguing possibility that MBD4 is epistatically related to the MMR pathway. The association of MBD4 with the MutLα heterodimer constituents MLH1 and PMS2 supports this view (17, 36). Residual CSR in our *Mbd4* KO cells presumably arises independently of MBD4 and the MMR pathway and may be due to endogenous UNG levels.

Analysis of S-S junctions is an excellent readout for the end-joining processes that ligate broken DNA ends (48). Two mechanistically distinct pathways are known to repair DSBs during CSR: classical NHEJ and alternative-end joining with long microhomologies (9). S-S junctions from B cells that lack the NHEJ component DNA ligase IV or XRCC4 contain long stretches of microhomology (>3 nt), characteristic of alternative-end joining (9). It has been noted that alternative-end joining may represent not a distinct pathway but rather a default pathway that arises when NHEJ components are absent (52). *Mbd4* deficiency resulted in Sμ-Sα junctions with longer microhomologies and fewer direct joins, a profile similar to those for *Mlh1*- or *Pms2*-deficient B cells (47). In contrast, *Msh2*-deficient B cells do not show increased junctional microhomologies, indicating that MMR pathway deficiencies may have different roles in DSB repair during CSR (48).

How might MBD4 function in the context of MMR and DSB formation? In the classical model of MMR-mediated DSB processing, there is recognition of U-G mismatches by MutSα/MutLα that cause complex activation and translocation along the DNA contour (Fig. 5B). Collision of PCNA loaded at a cleaved abasic site with the MutSα/MutLα complex activates MutLα endonucleolytic activity, which introduces additional nicks into the DNA strand (53). These nicks are used by ExoI as an entry site for the degradation of DNA in the 5′→3′ direction. ExoI removes the U-G mismatch and adjacent bases, creating a single-stranded gap, which, when opposite an SSB on the complementary strand, forms a DSB (Fig. 5Bc). A second model posits that assembly of the MutLα complex is an early event and that, once formed, the complex slides along DNA and contacts mismatch-activated MutSα, whereupon the MutLα endonuclease activity is activated (54). The key difference is that MutLα can independently slide along the DNA contour in the second model. This hypothesis is consistent with the finding that *Mlh1* has functions in CSR that are independent of *Msh2* (55). We suggest that the association of MBD4 with MutLα might allow MMR-dependent recognition of uracil residues and the creation of abasic sites via MBD4, which, in turn, triggers the recruitment of PCNA in a feed-forward mechanism leading to enhanced ExoI recruitment and increased DSB formation. In our proposal, MBD4 activity amplifies the creation of DSBs through the MMR pathway and increases the efficiency of CSR. More work is needed to verify key features of our proposal.

MATERIALS AND METHODS

Mice, cell culture, and proliferation assays. CH12.F3 cells were grown in culture, activated to undergo CSR by the addition of CD40L, IL-4, and TGF-β (CIT), and analyzed by FACS for surface IgA, as described previously (17). A subclone of CH12, C.24, was isolated by limiting dilution and was targeted by homologous recombination for deletion of *Mbd4* exons 6 to 8 and the 3′ UTR (Fig. S1A). C.24 and its sister clones (C.2, C.4) retain IgA switching frequencies similar to those of the parental bulk cultures, as assessed in FACS analyses (Fig. S1A and B). The C.24 subclone was further analyzed by limiting dilution,

and daughter subclones (C.24.1, C.24.5, and C.24.6) expressed similar CSR frequencies following CIT activation, indicating the stability of this phenotype (Fig. S1A and B). The CSR frequencies associated with subclones derived from 1A-12$^{\Delta/+}$ (1A-12$^{\Delta/+0.5}$, 1A-12$^{\Delta/+0.6}$) and 1A-12$^{\Delta/\Delta}$ (1A-12$^{\Delta/\Delta0.3}$, 1A-12$^{\Delta/\Delta0.4}$, 1A-12$^{\Delta/\Delta0.5}$) (with one exception, 1A-12$^{\Delta/+0.4}$), recapitulate the $\mu \rightarrow \alpha$ CSR frequency of their parental clones, 1A-12$^{N/+}$ and 1A-12$^{N/\Delta}$. CFSE (Invitrogen C1157) was used to assess cell proliferation, as described previously (56). Proliferation was monitored by flow cytometry analyses that include 10,000 to 15,000 events gated on live lymphoid cells using Cyan ADP (DakoCytomation) and Summit software (Becton, Dickinson). Mice were bred under specific-pathogen-free conditions in a fully accredited animal facility at the University of Illinois College of Medicine. All procedures involving mice were approved by the Institutional Animal Care Committee of the University of Illinois College of Medicine. *Mbd4*$^{\Delta2\text{-}5/\Delta2\text{-}5}$ mice were a kind gift from A. Bellacosa (Fox Chase) (16). Splenic B cells were isolated and activated with lipopolysaccharide (LPS) and IL-4 as described previously (57).

Western blotting, qRT-PCR, and microarray analyses. Cytoplasmic and nuclear extracts were prepared, and Western blot analyses were carried out, as described previously (17). An affinity-purified anti-AID Ab was generated (Anaspec) as described previously (58) and was further adsorbed using lysates from AID-deficient mice. qRT-PCR was performed as described previously (58) using primers for 18S RNA (59) and AID (57), primers GLTμ-F (5′-CTCTGGCCCTGCTTATTGTTG-3′) and GLTμ-R (5′-GAAGACATTTGG GAAGGACTGACT-3′), and primers GLTα-F (5′-CCTGGCTGTTCCCCTATGAA-3′) and GLTα-R (5′-CGGAAGG GAAGTAATCGTGA-3′). *Mbd4* primers were F1 and R1 (14), R2 (5′-ATGCATCACCACACAGCTAACAGAAT-3′), R3 (5′-AGGGGTCCATTTCTTGAAGG-3′), F4 (5′-ACCAAAGCTGCCTTCACACT-3′) and R4 (5′-TCCTTTGTTCCT TGCCCAAC-3′), R5 (5′-CCATGAAGCTCAATCGGATACC-3′), F6.1 (5′-CACCGAAGTGGCCCGAGCTGC CGAC), and R8.1 (5′-TCA AGA TAG ACT TAA TTT TTC ATG ATT-3′). For microarray analyses, control or *Mbd4* KO cells were CIT activated for 24 h; two independent mRNA samples from each cell type were purified using the RNeasy MinElute cleanup kit (catalog no. 74204; Qiagen); and cDNAs were synthesized and hybridized to Mouse Gene 1.0 ST arrays (catalog no. 901171; Affymetrix) according to the manufacturer's instructions. Hybridization signal intensities were normalized by quantiles and were summarized using the robust multiarray average (RMA) method. Data were analyzed using the Partek, Inc., Genomics Suite statistical package and are available in the GEO database (GEO accession no. GSE51559).

Accession number(s). Microarray data comparing gene expression in CH12 control cells with that in *Mbd4* KO cells have been deposited in the Gene Expression Omnibus (GEO) database (http://www.ncbi.nlm.nih.gov/geo/) under accession number GSE51559.

SUPPLEMENTAL MATERIAL

Supplemental material for this article may be found at https://doi.org/10.1128/MCB.00316-16.

TEXT S1, PDF file, 1.5 MB.

ACKNOWLEDGMENTS

We thank the UIC Research Resources Center Genomics lab for expert microarray analyses, J. Stavnezer and C. Schrader (University of Massachusetts) for the compendium of DSBs from B cells, F. Alt (Harvard) for pLNTK, and A. Bellacosa (Fox Chase) for *Mbd4*$^{\Delta2\text{-}5/\Delta2\text{-}5}$ mice. We thank J. Stavnezer for critical reading of the manuscript and H. Shen for expert technical help.

We declare no competing financial interests.

REFERENCES

1. Chaudhuri J, Basu U, Zarrin A, Yan C, Franco S, Perlot T, Vuong B, Wang J, Phan RT, Datta A, Manis J, Alt FW. 2007. Evolution of the immunoglobulin heavy chain class switch recombination mechanism. Adv Immunol 94:157–214. https://doi.org/10.1016/S0065-2776(06)94006-1.
2. Kenter AL. 2012. AID targeting is dependent on RNA polymerase II pausing. Semin Immunol 24:281–286. https://doi.org/10.1016/j.smim.2012.06.001.
3. Feldman S, Achour I, Wuerffel R, Kumar S, Gerasimova T, Sen R, Kenter AL. 2015. Constraints contributed by chromatin looping limit recombination targeting during Ig class switch recombination. J Immunol 194:2380–2389. https://doi.org/10.4049/jimmunol.1401170.
4. Matthews AJ, Zheng S, DiMenna LJ, Chaudhuri J. 2014. Regulation of immunoglobulin class-switch recombination: choreography of noncoding transcription, targeted DNA deamination, and long-range DNA repair. Adv Immunol 122:1–57. https://doi.org/10.1016/B978-0-12-800267-4.00001-8.
5. Rada C, Williams GT, Nilsen H, Barnes DE, Lindahl T, Neuberger MS. 2002. Immunoglobulin isotype switching is inhibited and somatic hypermutation perturbed in UNG-deficient mice. Curr Biol 12:1748–1755. https://doi.org/10.1016/S0960-9822(02)01215-0.
6. Stavnezer J, Guikema JE, Schrader CE. 2008. Mechanism and regulation of class switch recombination. Annu Rev Immunol 26:261–292. https://doi.org/10.1146/annurev.immunol.26.021607.090248.
7. Durandy A, Peron S, Fischer A. 2006. Hyper-IgM syndromes. Curr Opin Rheumatol 18:369–376. https://doi.org/10.1097/01.bor.0000231905.12172.b5.
8. Schrader CE, Guikema JE, Linehan EK, Selsing E, Stavnezer J. 2007. Activation-induced cytidine deaminase-dependent DNA breaks in class switch recombination occur during G_1 phase of the cell cycle and depend upon mismatch repair. J Immunol 179:6064–6071. https://doi.org/10.4049/jimmunol.179.9.6064.
9. Yan CT, Boboila C, Souza EK, Franco S, Hickernell TR, Murphy M, Gumaste S, Geyer M, Zarrin AA, Manis JP, Rajewsky K, Alt FW. 2007. IgH class switching and translocations use a robust non-classical end-joining pathway. Nature 449:478–482. https://doi.org/10.1038/nature06020.
10. Schrader CE, Linehan EK, Mochegova SN, Woodland RT, Stavnezer J. 2005. Inducible DNA breaks in Ig S regions are dependent on AID and UNG. J Exp Med 202:561–568. https://doi.org/10.1084/jem.20050872.
11. Visnes T, Doseth B, Pettersen HS, Hagen L, Sousa MM, Akbari M, Otterlei M, Kavli B, Slupphaug G, Krokan HE. 2009. Uracil in DNA and its pro-

cessing by different DNA glycosylases. Philos Trans R Soc Lond B Biol Sci 364:563–568. https://doi.org/10.1098/rstb.2008.0186.
12. Di Noia JM, Rada C, Neuberger MS. 2006. SMUG1 is able to excise uracil from immunoglobulin genes: insight into mutation versus repair. EMBO J 25:585–595. https://doi.org/10.1038/sj.emboj.7600939.
13. Di Noia JM, Williams GT, Chan DT, Buerstedde JM, Baldwin GS, Neuberger MS. 2007. Dependence of antibody gene diversification on uracil excision. J Exp Med 204:3209–3219. https://doi.org/10.1084/jem.20071768.
14. Dingler FA, Kemmerich K, Neuberger MS, Rada C. 2014. Uracil excision by endogenous SMUG1 glycosylase promotes efficient Ig class switching and impacts on A:T substitutions during somatic mutation. Eur J Immunol 44:1925–1935. https://doi.org/10.1002/eji.201444482.
15. Rai K, Huggins IJ, James SR, Karpf AR, Jones DA, Cairns BR. 2008. DNA demethylation in zebrafish involves the coupling of a deaminase, a glycosylase, and gadd45. Cell 135:1201–1212. https://doi.org/10.1016/j.cell.2008.11.042.
16. Cortellino S, Turner D, Masciullo V, Schepis F, Albino D, Daniel R, Skalka AM, Meropol NJ, Alberti C, Larue L, Bellacosa A. 2003. The base excision repair enzyme MED1 mediates DNA damage response to antitumor drugs and is associated with mismatch repair system integrity. Proc Natl Acad Sci U S A 100:15071–15076. https://doi.org/10.1073/pnas.2334585100.
17. Grigera F, Bellacosa A, Kenter AL. 2013. Complex relationship between mismatch repair proteins and MBD4 during immunoglobulin class switch recombination. PLoS One 8:e78370. https://doi.org/10.1371/journal.pone.0078370.
18. Bellacosa A. 2001. Functional interactions and signaling properties of mammalian DNA mismatch repair proteins. Cell Death Differ 8:1076–1092. https://doi.org/10.1038/sj.cdd.4400948.
19. Bardwell PD, Martin A, Wong E, Li Z, Edelmann W, Scharff MD. 2003. The G-U mismatch glycosylase methyl-CpG binding domain 4 is dispensable for somatic hypermutation and class switch recombination. J Immunol 170:1620–1624. https://doi.org/10.4049/jimmunol.170.4.1620.
20. Hendrich B, Abbott C, McQueen H, Chambers D, Cross S, Bird A. 1999. Genomic structure and chromosomal mapping of the murine and human Mbd1, Mbd2, Mbd3, and Mbd4 genes. Mamm Genome 10:906–912. https://doi.org/10.1007/s003359901112.
21. Hashimoto H, Zhang X, Cheng X. 2012. Excision of thymine and 5-hydroxymethyluracil by the MBD4 DNA glycosylase domain: structural basis and implications for active DNA demethylation. Nucleic Acids Res 40:8276–8284. https://doi.org/10.1093/nar/gks628.
22. Heintzman ND, Stuart RK, Hon G, Fu Y, Ching CW, Hawkins RD, Barrera LO, Van Calcar S, Qu C, Ching KA, Wang W, Weng Z, Green RD, Crawford GE, Ren B. 2007. Distinct and predictive chromatin signatures of transcriptional promoters and enhancers in the human genome. Nat Genet 39:311–318. https://doi.org/10.1038/ng1966.
23. Creyghton MP, Cheng AW, Welstead GG, Kooistra T, Carey BW, Steine EJ, Hanna J, Lodato MA, Frampton GM, Sharp PA, Boyer LA, Young RA, Jaenisch R. 2010. Histone H3K27ac separates active from poised enhancers and predicts developmental state. Proc Natl Acad Sci U S A 107:21931–21936. https://doi.org/10.1073/pnas.1016071107.
24. Kagey MH, Newman JJ, Bilodeau S, Zhan Y, Orlando DA, van Berkum NL, Ebmeier CC, Goossens J, Rahl PB, Levine SS, Taatjes DJ, Dekker J, Young RA. 2010. Mediator and cohesin connect gene expression and chromatin architecture. Nature 467:430–435. https://doi.org/10.1038/nature09380.
25. Muramatsu M, Sankaranand VS, Anant S, Sugai M, Kinoshita K, Davidson NO, Honjo T. 1999. Specific expression of activation-induced cytidine deaminase (AID), a novel member of the RNA-editing deaminase family in germinal center B cells. J Biol Chem 274:18470–18476. https://doi.org/10.1074/jbc.274.26.18470.
26. Han L, Yu K. 2008. Altered kinetics of nonhomologous end joining and class switch recombination in ligase IV-deficient B cells. J Exp Med 205:2745–2753. https://doi.org/10.1084/jem.20081623.
27. Masani S, Han L, Yu K. 2013. Apurinic/apyrimidinic endonuclease 1 is the essential nuclease during immunoglobulin class switch recombination. Mol Cell Biol 33:1468–1473. https://doi.org/10.1128/MCB.00026-13.
28. Han L, Mao W, Yu K. 2012. X-ray repair cross-complementing protein 1 (XRCC1) deficiency enhances class switch recombination and is permissive for alternative end joining. Proc Natl Acad Sci U S A 109:4604–4608. https://doi.org/10.1073/pnas.1120743109.
29. Han L, Masani S, Yu K. 2010. CTNNBL1 is dispensable for Ig class switch recombination. J Immunol 185:1379–1381. https://doi.org/10.4049/jimmunol.1001643.
30. Han L, Masani S, Hsieh CL, Yu K. 2014. DNA ligase I is not essential for mammalian cell viability. Cell Rep 7:316–320. https://doi.org/10.1016/j.celrep.2014.03.024.
31. Sternberg N, Hoess R. 1983. The molecular genetics of bacteriophage P1. Annu Rev Genet 17:123–154. https://doi.org/10.1146/annurev.ge.17.120183.001011.
32. Rush JS, Hasbold J, Hodgkin PD. 2002. Cross-linking surface Ig delays CD40 ligand- and IL-4-induced B cell Ig class switching and reveals evidence for independent regulation of B cell proliferation and differentiation. J Immunol 168:2676–2682. https://doi.org/10.4049/jimmunol.168.6.2676.
33. Bader SA, Walker M, Harrison DJ. 2007. A human cancer-associated truncation of MBD4 causes dominant negative impairment of DNA repair in colon cancer cells. Br J Cancer 96:660–666. https://doi.org/10.1038/sj.bjc.6603592.
34. Ran FA, Hsu PD, Wright J, Agarwala V, Scott DA, Zhang F. 2013. Genome engineering using the CRISPR-Cas9 system. Nat Protoc 8:2281–2308. https://doi.org/10.1038/nprot.2013.143.
35. Jinek M, Chylinski K, Fonfara I, Hauer M, Doudna JA, Charpentier E. 2012. A programmable dual-RNA-guided DNA endonuclease in adaptive bacterial immunity. Science 337:816–821. https://doi.org/10.1126/science.1225829.
36. Bellacosa A, Cicchillitti L, Schepis F, Riccio A, Yeung AT, Matsumoto Y, Golemis EA, Genuardi M, Neri G. 1999. MED1, a novel human methyl-CpG-binding endonuclease, interacts with DNA mismatch repair protein MLH1. Proc Natl Acad Sci U S A 96:3969–3974. https://doi.org/10.1073/pnas.96.7.3969.
37. Wuerffel RA, Du J, Thompson RJ, Kenter AL. 1997. Ig Sγ3 DNA-specific double strand breaks are induced in mitogen-activated B cells and are implicated in switch recombination. J Immunol 159:4139–4144.
38. Di Noia JM, Neuberger MS. 2007. Molecular mechanisms of antibody somatic hypermutation. Annu Rev Biochem 76:1–22. https://doi.org/10.1146/annurev.biochem.76.061705.090740.
39. Schrader CE, Guikema JE, Wu X, Stavnezer J. 2009. The roles of APE1, APE2, DNA polymerase beta and mismatch repair in creating S region DNA breaks during antibody class switch. Philos Trans R Soc Lond B Biol Sci 364:645–652. https://doi.org/10.1098/rstb.2008.0200.
40. Bregenhorn S, Kallenberger L, Artola-Boran M, Pena-Diaz J, Jiricny J. 2016. Non-canonical uracil processing in DNA gives rise to double-strand breaks and deletions: relevance to class switch recombination. Nucleic Acids Res 44:2691–2705. https://doi.org/10.1093/nar/gkv1535.
41. Xue K, Rada C, Neuberger MS. 2006. The in vivo pattern of AID targeting to immunoglobulin switch regions deduced from mutation spectra in msh2$-/-$ ung$-/-$ mice. J Exp Med 203:2085–2094. https://doi.org/10.1084/jem.20061067.
42. Rush JS, Fugmann SD, Schatz DG. 2004. Staggered AID-dependent DNA double strand breaks are the predominant DNA lesions targeted to S mu in Ig class switch recombination. Int Immunol 16:549–557. https://doi.org/10.1093/intimm/dxh057.
43. Wang L, Wuerffel R, Feldman S, Khamlichi AA, Kenter AL. 2009. S region sequence, RNA polymerase II, and histone modifications create chromatin accessibility during class switch recombination. J Exp Med 206:1817–1830. https://doi.org/10.1084/jem.20081678.
44. Daniel JA, Santos MA, Wang Z, Zang C, Schwab KR, Jankovic M, Filsuf D, Chen HT, Gazumyan A, Yamane A, Cho YW, Sun HW, Ge K, Peng W, Nussenzweig MC, Casellas R, Dressler GR, Zhao K, Nussenzweig A. 2010. PTIP promotes chromatin changes critical for immunoglobulin class switch recombination. Science 329:917–923. https://doi.org/10.1126/science.1187942.
45. Min IM, Rothlein LR, Schrader CE, Stavnezer J, Selsing E. 2005. Shifts in targeting of class switch recombination sites in mice that lack mu switch region tandem repeats or Msh2. J Exp Med 201:1885–1890. https://doi.org/10.1084/jem.20042491.
46. Ehrenstein MR, Neuberger MS. 1999. Deficiency in Msh2 affects the efficiency and local sequence specificity of immunoglobulin class-switch recombination: parallels with somatic hypermutation. EMBO J 18:3484–3490. https://doi.org/10.1093/emboj/18.12.3484.
47. Schrader CE, Vardo J, Stavnezer J. 2002. Role for mismatch repair proteins Msh2, Mlh1, and Pms2 in immunoglobulin class switching shown by sequence analysis of recombination junctions. J Exp Med 195:367–373. https://doi.org/10.1084/jem.20011877.
48. Stavnezer J, Bjorkman A, Du L, Cagigi A, Pan-Hammarstrom Q. 2010. Mapping of switch recombination junctions, a tool for studying DNA repair pathways during immunoglobulin class switching. Adv

Immunol 108:45–109. https://doi.org/10.1016/B978-0-12-380995-7.00003-3.
49. Sjolund AB, Senejani AG, Sweasy JB. 2013. MBD4 and TDG: multifaceted DNA glycosylases with ever expanding biological roles. Mutat Res 743–744:12–25. https://doi.org/10.1016/j.mrfmmm.2012.11.001.
50. Screaton RA, Kiessling S, Sansom OJ, Millar CB, Maddison K, Bird A, Clarke AR, Frisch SM. 2003. Fas-associated death domain protein interacts with methyl-CpG binding domain protein 4: a potential link between genome surveillance and apoptosis. Proc Natl Acad Sci U S A 100:5211–5216. https://doi.org/10.1073/pnas.0431215100.
51. Ruzov A, Shorning B, Mortusewicz O, Dunican DS, Leonhardt H, Meehan RR. 2009. MBD4 and MLH1 are required for apoptotic induction in xDNMT1-depleted embryos. Development 136:2277–2286. https://doi.org/10.1242/dev.032227.
52. Lieber MR. 2010. The mechanism of double-strand DNA break repair by the nonhomologous DNA end-joining pathway. Annu Rev Biochem 79:181–211. https://doi.org/10.1146/annurev.biochem.052308.093131.
53. Iyer RR, Pluciennik A, Burdett V, Modrich PL. 2006. DNA mismatch repair: functions and mechanisms. Chem Rev 106:302–323. https://doi.org/10.1021/cr0404794.
54. Kadyrova LY, Kadyrov FA. 2016. Endonuclease activities of MutLalpha and its homologs in DNA mismatch repair. DNA Repair (Amst) 38:42–49. https://doi.org/10.1016/j.dnarep.2015.11.023.
55. Schrader CE, Vardo J, Stavnezer J. 2003. Mlh1 can function in antibody class switch recombination independently of Msh2. J Exp Med 197:1377–1383. https://doi.org/10.1084/jem.20022190.
56. Nowak U, Matthews AJ, Zheng S, Chaudhuri J. 2011. The splicing regulator PTBP2 interacts with the cytidine deaminase AID and promotes binding of AID to switch-region DNA. Nat Immunol 12:160–166. https://doi.org/10.1038/ni.1977.
57. Wuerffel R, Wang L, Grigera F, Manis J, Selsing E, Perlot T, Alt FW, Cogne M, Pinaud E, Kenter AL. 2007. S-S synapsis during class switch recombination is promoted by distantly located transcriptional elements and activation-induced deaminase. Immunity 27:711–722. https://doi.org/10.1016/j.immuni.2007.09.007.
58. Kumar S, Wuerffel R, Achour I, Lajoie B, Sen R, Dekker J, Feeney AJ, Kenter AL. 2013. Flexible ordering of antibody class switch and V(D)J joining during B-cell ontogeny. Genes Dev 27:2439–2444. https://doi.org/10.1101/gad.227165.113.
59. Rhinn H, Marchand-Leroux C, Croci N, Plotkine M, Scherman D, Escriou V. 2008. Housekeeping while brain's storming: validation of normalizing factors for gene expression studies in a murine model of traumatic brain injury. BMC Mol Biol 9:62. https://doi.org/10.1186/1471-2199-9-62.